

1 **Longitudinal conjunction between MESSENGER and**  
2 **STEREO A: development of ICME complexity**  
3 **through stream interactions**

Reka M. Winslow,<sup>1</sup> Noé Lugaz,<sup>1</sup> Nathan A. Schwadron,<sup>1</sup> Charles J.

Farrugia,<sup>1</sup> Wenyuan Yu,<sup>1</sup> Jim M. Raines,<sup>2</sup> M. Leila Mays,<sup>3,4</sup> Antoinette B.

Galvin,<sup>1</sup> and Thomas H. Zurbuchen<sup>2</sup>

---

Corresponding author: Reka M. Winslow, Institute for the Study of Earth, Ocean, and Space,  
University of New Hampshire, Durham, New Hampshire, USA. (reka.winslow@unh.edu)

<sup>1</sup>Institute for the Study of Earth, Ocean,  
and Space, University of New Hampshire,  
Durham, New Hampshire, USA.

<sup>2</sup>Department of Climate and Space  
Sciences and Engineering, University of  
Michigan, Ann Arbor MI, USA.

<sup>3</sup>Catholic University of America,  
Washington, DC, USA.

<sup>4</sup>Heliophysics Science Division, NASA  
Goddard Space Flight Center, Greenbelt,  
MD, USA.

**This is the author manuscript accepted for publication and has undergone full peer review but has not been through the copyediting, typesetting, pagination and proofreading process, which may lead to differences between this version and the Version of Record. Please cite this article**

as doi:10.1002/2015JA022307 June 23, 2016, 5:59am

D R A F T

**4 Abstract.**

5 We use data on an interplanetary coronal mass ejection (ICME) seen by  
6 MESSENGER and STEREO A starting on 29 December 2011 in a near-perfect  
7 longitudinal conjunction (within  $3^\circ$ ) to illustrate changes in its structure via  
8 interactions with the solar wind in less than 0.6 AU. From force-free field mod-  
9 eling we infer that the orientation of the underlying flux rope has undergone  
10 a rotation of  $\sim 80^\circ$  in latitude and  $\sim 65^\circ$  in longitude. Based on both space-  
11 craft measurements as well as ENLIL model simulations of the steady state  
12 solar wind, we find that interaction involving magnetic reconnection with coro-  
13 tating structures in the solar wind dramatically alters the ICME magnetic  
14 field. In particular, we observed a highly turbulent region with distinct prop-  
15 erties within the flux rope at STEREO A, not observed at MESSENGER,  
16 which we attribute to interaction between the ICME and a heliospheric plasma  
17 sheet/current sheet during propagation. Our case study is a concrete exam-  
18 ple of a sequence of events that can increase the complexity of ICMEs with  
19 heliocentric distance even in the inner heliosphere. The results highlight the  
20 need for large scale statistical studies of ICME events observed in conjunc-  
21 tion at different heliocentric distances to determine how frequently signif-  
22 icant changes in flux rope orientation occur during propagation. These re-  
23 sults also have significant implications for space weather forecasting and should  
24 serve as a caution on using very distant observations to predict the geoeff-  
25 ectiveness of large interplanetary transients.

## 1. Introduction

26 Coronal mass ejections (CMEs) are large eruptions of plasma and magnetic field into  
27 interplanetary space originating in the Sun's atmosphere [e.g., Cane & Richardson, 2003;  
28 Zurbuchen & Richardson, 2006]. The interplanetary counterparts of CMEs are known as  
29 interplanetary coronal mass ejections (ICMEs) and fast ICMEs are most often character-  
30 ized by a leading shock wave followed by a dense sheath and a magnetic flux rope at the  
31 center of the disturbance. ICMEs are common, passing over Earth at an approximate rate  
32 of 1-2 per month [Lynch et al., 2003; Richardson & Cane, 2010], although this number is  
33 significantly higher near the maximum phase of the solar cycle.

34 At Earth, the effects of ICMEs on the magnetosphere have been studied for many  
35 decades [e.g., review by Singh et al., 2010]. Because ICMEs can be associated with strong  
36 southward interplanetary magnetic fields of long duration, high solar wind velocities,  
37 enhanced solar wind dynamic pressures, and solar energetic particles, they are strong  
38 drivers of geomagnetic storm activity at Earth [e.g., Lindsay et al., 1995; Farrugia et al.,  
39 1997]. Geomagnetic storms are caused by the transfer of momentum and energy from  
40 the solar wind to the magnetosphere during times of southward-directed interplanetary  
41 magnetic fields, when magnetic reconnection can occur between the oppositely directed  
42 fields of the interplanetary magnetic field (IMF) and Earth [e.g., Russell et al., 1974;  
43 Farrugia et al., 1993]. Using space-based observations, Gonzalez & Tsurutani [1987] have  
44 shown that ICMEs with southward-pointed magnetic fields greater than 10 nT and lasting  
45 longer than approximately 3 hours lead to intense ( $Dst < -100$  nT) magnetic storms, where  
46 the Dst index is a measure of the strength of the ring current around the Earth.

47 The geoeffectiveness, or the storm-causing ability, of ICMEs strongly depends on the  
48 magnetic field direction within them. ICMEs are strong drivers of geomagnetic activity, as  
49 a statistical study by Zhang et al. [2004] showed that 70% of intense storms are caused by  
50 ICMEs. However, only about 20% of Earth directed solar ejecta cause intense geomagnetic  
51 storms [Tsunobuchi et al., 1988]. The rest either do not have substantial southward-directed  
52 fields or have highly time-varying magnetic fields, i.e., do not have strong southward-  
53 directed fields for more than 3 hours. Thus, successfully predicting the occurrence and  
54 intensity of geomagnetic storms based on magnetic field measurements relies on the ability  
55 to measure the orientation of the magnetic field in the ICME and its duration prior to  
56 it reaching Earth, provided that the magnetic field direction does not change drastically  
57 during the remaining propagation time. A recent proof-of-concept study by Kubicka et  
58 al. [2016] based on one ICME event shows that such predictions are possible, although  
59 further work is needed to establish the conditions under which they are valid.

60 ICME properties can change drastically as the ICME propagates through the solar  
61 wind. Temperature, density, pressure, magnetic field, and shock structure can all change as  
62 the ICME expands and interacts both with the ambient solar wind as well as with various  
63 disturbances within it. In particular, through observational and modeling work, studies  
64 have shown that during propagation the flux rope may kink and deform [Manchester et  
65 al., 2004], reconnection/erosion of internal ICME magnetic flux may occur [Lavraud et  
66 al., 2014; Puffenach et al., 2015], and the ICME may also get deflected [Manchester et al.,  
67 2005; Kay et al., 2013, 2015; Wang et al., 2014] and rotated [Kliem et al., 2012; Lynch et  
68 al., 2009]. A recent CME event study by Nieves-Chinchilla et al. [2012] using both in situ  
69 and remote sensing observations from STEREO, SOHO, MESSENGER and Wind showed

70 evidence for significant re-orientation of the flux rope axis. Similarly, Rouillard et al. [2009]  
71 showed that the trailing part of a particular ICME displayed highly distinct magnetic  
72 signatures at MESSENGER compared to measurements at Venus Express, despite the  
73 very small ( $\sim 1^\circ$ ) longitudinal separation between the two spacecraft. On the other hand,  
74 an in situ study by Good et al. [2015] of an ICME observed in near-perfect conjunction  
75 at Mercury and STEREO B has showcased an event where the large-scale magnetic field  
76 structure evolution in the magnetic cloud (MC) remains self-similar during propagation.  
77 In situ multipoint measurements by Möstl et al. [2012] of a series of ICME events also  
78 show similarities between the flux ropes observed by Venus Express and STEREO B,  
79 despite the  $\sim 18^\circ$  longitudinal separation between the spacecraft.

80 The varied results of these studies raise the question: what causes some ICME flux  
81 ropes to change drastically during propagation while others stay relatively self-similar?  
82 These past works therefore highlight the need for further exploration of evolution of the  
83 ICME magnetic field structure during propagation. Now, with 5 years of MESSENGER  
84 measurements near Mercury's orbit as well as continuous spacecraft measurements at 1  
85 AU, such studies are possible for the first time in the innermost heliosphere. Also, a new  
86 era of inner heliosphere exploration from in situ measurements is expected to begin with  
87 the launch of Solar Orbiter [Müller & St. Cyr, 2013] and Solar Probe Plus [Fox et al.,  
88 2015] in the next three years. Due to their proximity to the Sun, these spacecraft (will)  
89 present a unique opportunity for observing ICMEs in more "pristine" conditions, well  
90 before they reach 1 AU.

91 In this paper we present a study of a CME launched from the Sun on 29 December 2011,  
92 and we follow its propagation from the Sun to 1 AU. Due to the MESSENGER / STEREO

93 A directed nature of the ICME, and the near-perfect alignment between these spacecraft at  
94 this time, one would expect close agreement of flux rope parameters at the two locations.  
95 Instead, due to the interaction of the ICME with the heliospheric plasma sheet (HPS) and  
96 current sheet (HCS) between Mercury and STEREO A, a very different ICME magnetic  
97 field structure was observed at the two spacecraft. The observations and analyses present a  
98 concrete example of a scenario where ICME interaction with corotating structures in the  
99 solar wind significantly alters the flux rope magnetic topology and increases the complexity  
100 of the ICME during propagation. Based on these results, our paper is a caution on using  
101 magnetic field measurements close to the Sun for geomagnetic storm forecasting at Earth  
102 when corotating structures are present in the Sun-to-Earth transit space. Large-scale  
103 statistical studies of ICME magnetic field changes from the innermost heliosphere to 1  
104 AU are also necessary to determine the frequency with which drastic alterations in flux  
105 rope orientation occur due to solar wind interactions.

## 2. 29 December 2011 CME

106 The CME was launched from the Sun at or around 15:52 UT on 29 December 2011 and  
107 was observed by coronagraphs onboard both STEREOs and SOHO. STEREO A EUVI  
108 observations show a filament eruption from disk center with the rising phase starting  
109 around 15:00 UT. At this time, STEREO A was  $\sim 107^\circ$  west of the Sun-Earth line while  
110 STEREO B was  $\sim 111^\circ$  east of the Sun-Earth line. The first observation by STEREO  
111 A/COR-2 of the CME was at 17:24 UT and appeared as a front halo CME, i.e. it  
112 was directed at STEREO A. The same event was also observed as a back-sided halo by  
113 STEREO-B/COR2. SOHO/LASCO observed a wide western limb CME (first image 16:24  
114 UT). Since it is a limb CME for LASCO, this instrument provides the best estimate of

115 the CME onset and speed, 15:52 UT and  $750 \text{ km s}^{-1}$ , respectively. The COR-2 maximum  
116 speeds were  $540$  and  $780 \text{ km s}^{-1}$  for STEREO A and B, respectively.

117 Due to the near-perfect alignment (within  $3^\circ$  longitude) of MESSENGER and STEREO  
118 A between the time of the CME launch on 29 December 2011 and its arrival at STEREO  
119 A on 1 January 2012, the CME was observed in situ at both spacecraft. At this time,  
120 Mercury's heliocentric distance was  $0.42 \text{ AU}$ , while the STEREO A heliocentric distance  
121 was  $0.96 \text{ AU}$ . With a speed of  $750 \text{ km s}^{-1}$ , and assuming no deceleration, this CME  
122 would arrive at Mercury 23 hours after its launch, or at  $\sim 14:50 \text{ UT}$  on December 30,  
123 and at  $\sim 21:00 \text{ UT}$  on December 31 at STEREO A. Taking into account uncertainties  
124 in the estimated speed and the expected deceleration of the CME in the solar wind,  
125 this CME has the required timing characteristics to correspond to the ICME and shock  
126 measured at MESSENGER on December 30 starting at 16:27 UT ( $\sim 1.5$  hours “late”) and  
127 to correspond to the ICME measured at STEREO A arriving at 13:22 UT ( $\sim 16.5$  hours  
128 “late”) on January 1st. We note that these arrival timing differences are quite minor given  
129 the assumption of constant velocity. Additionally, we perform a more complete analysis  
130 of the CME kinematics at the end of Section 3.

131 The graduated cylindrical shell (GCS) model [Thernisien et al., 2006, 2011] was designed  
132 to reproduce the large-scale structure of flux rope-like CMEs and determines the initial  
133 orientation of the flux rope soon after launch. To this end, we use the GCS fit from  
134 the STEREO/SECCHI/COR2 CME Kinematic Database (KINCAT) of the Institute for  
135 Astrophysics, University of Göttingen, Germany. The database is available online at  
136 <http://www.affects-fp7.eu/helcats-database>. The GCS fit of this CME as seen  
137 from STEREO A (Figure 1a) and B (Figure 1b) SECCHI data (using white light images

138 from December 29 at 19:08 UT) finds that the flux rope longitude was  $98^\circ \pm 4^\circ$ , the  
139 latitude was  $7^\circ \pm 2^\circ$ , with a tilt angle of  $-36^\circ \pm 22^\circ$ . At this time, STEREO A was at  
140 a longitude of  $107^\circ$ , so this implies that the CME initial flux rope orientation was only  
141  $9^\circ$  away from the Sun - MESSENGER - STEREO A line, towards the east, i.e. towards  
142 the Sun - Earth line. These results forecast the CME to be hitting MESSENGER and  
143 STEREO A nearly head-on.

144 (i) The longitudinal alignment between MESSENGER and STEREO A, (ii) the initial  
145 direction of the CME determined to be within  $\sim 10^\circ$  of STEREO A, (iii) the arrival time  
146 of the ICME matching quite closely with the expected arrival times at the two spacecraft,  
147 and (iv) the same chirality of the flux rope observed at the two spacecraft (see Section 3  
148 below) all support the hypothesis that the measurements at MESSENGER and STEREO  
149 A are of the same ICME. Using the method of coplanarity [e.g., Schwartz, 1998], we have  
150 determined the shock normal direction in heliospheric radial-tangential-normal (RTN)  
151 coordinates at both spacecraft and found  $\hat{n} = (0.77, 0.20, 0.61)$  at MESSENGER and  $\hat{n}$   
152  $= (0.71, 0.18, 0.68)$  at STEREO A, yielding a  $5^\circ$  difference between the two shock normal  
153 directions. The very close agreement between the shock normals provides further evidence  
154 that the measurements at the two spacecraft are of the same ICME.

## 2.1. MESSENGER Data

155 At Mercury, the ICME was observed in MESSENGER magnetic field data. Due to its  
156 highly eccentric orbit, during this time MESSENGER typically spent 8-10 hours of its 12  
157 hour orbit in the interplanetary medium. Magnetometer sample rates in the interplanetary  
158 medium were at least as high as 2 samples/s and a channel to record fluctuations at 1-10  
159 Hz operated continuously to provide an uninterrupted measure of the field variability.



160 Although the MESSENGER payload included a plasma spectrometer [the Fast Imaging  
161 Plasma Spectrometer (FIPS), see Andrews et al., 2007], the spacecraft was three axis  
162 stabilized and FIPS had a limited field of view that did not allow for the recovery of  
163 the solar wind density. Solar wind speed and temperature could be derived from the  
164 measurements about 50% of the time that MESSENGER was in the solar wind [Gershman  
165 et al., 2012].

166 In Winslow et al. [2015] we describe in detail the strict selection criteria used to identify  
167 ICME events from only magnetic field measurements. Due to the strong magnetic field and  
168 shock associated with this ICME and the smooth magnetic field rotation in the magnetic  
169 ejecta (ME), an ICME is easily discernible in the data. Figure 2 shows the ICME event in  
170 the MESSENGER magnetic field data, displayed in RTN coordinates. The ICME shock  
171 arrived on December 30th at 16:27:23 UT (first magenta vertical line in Figure 2), followed  
172 by the sheath region and ME. The ME start time of 20:52:38 UT is  $\sim 3$  hours later than our  
173 initial choice shown in Winslow et al. [2015], yielding a total sheath crossing time of  $\sim 5$   
174 hours (highlighted by the first two vertical magenta guidelines). After careful consideration,  
175 in light of partial FIPS data of the solar wind, we revised the start of the ME such that  
176 the sheath still includes the highly turbulent region between  $\sim 19:45$  and  $\sim 20:50$  UT. A  
177 simple analysis of the magnetic field latitude vs. longitude shows that this turbulent  
178 region exhibits a very clear planar structure (i.e. the magnetic field varies strictly in a  
179 plane), which is expected for ICME sheaths [Palmerio et al., 2016]. Furthermore, the last  
180 panel in Figure 2 shows a fairly steady cumulative proton count from the time of the  
181 ICME arrival until  $\sim 20:45$  UT, at which time there was a distinct and sustained drop in  
182 the flux coinciding quite closely in time with the beginning of the smooth magnetic field

183 rotation, signaling a transition from ICME sheath to ME. MESSENGER then crossed  
184 Mercury's magnetosphere between 22:25:12 UT and 01:12:02 UT on December 31. Once  
185 MESSENGER re-emerged into the interplanetary medium, the proton flux was still low,  
186 in agreement with the magnetic field measurements that MESSENGER was once again in  
187 the ME part of the ICME. The magnetic field in this ICME flux rope is characterized  
188 by low magnetic fluctuations, and a rotation of the magnetic field vector is observed in  
189 the  $B_T$  and  $B_N$  components, with  $B_T$  being the dominant field component in the ME.  
190 The end of the ME at 09:19:52 UT (last vertical magenta line in Figure 2) was marked  
191 by a discontinuity, possibly a weak reverse shock.

## 2.2. STEREO A Data

192 In this section, our aim is to focus on STEREO A data of the ICME only, while in  
193 Section 4, we discuss at length the STEREO A measurements prior to the ICME, as well  
194 as the background solar wind both from data and simulations. At 1 AU, STEREO A data  
195 show the ICME to be significantly more disturbed than at MESSENGER. The IMPACT  
196 [Luhmann et al., 2008] and PLASTIC [Galvin et al., 2008] packages on the STEREO  
197 spacecraft were specifically designed to provide in situ measurements of ICMEs including  
198 magnetic field observations and 3-D distributions of the solar wind plasma. Figure 3  
199 shows STEREO A data (magnetic field, suprathermal electron pitch angle distributions,  
200 density, velocity, temperature, plasma  $\beta$ , and the iron charge state distribution) of the  
201 ICME. Suprathermal electron pitch angle distributions have been normalized at each time  
202 step, and represent cumulative electron fluxes over all energies between 45 - 2188 eV. Iron  
203 charge state data are accumulated in 10 minute intervals, plotted at the beginning of the  
204 interval. The ICME shock arrival at 13:23:44 UT on 1 January 2012 is marked by a clear

205 jump in the magnetic field magnitude, coincident with jumps in plasma density, velocity,  
206 and temperature. Then STEREO A spent  $\sim 8.6$  hours in the ICME sheath (between the  
207 first two magenta vertical guidelines in Figure 3) where the magnetic field strength and  
208 direction were highly variable. The suprathermal electron pitch angle distributions exhibit  
209 an abrupt change from the  $180^\circ$  strahl component to uni-directional flows in the opposite  
210 direction at the shock, followed by mostly uni-directional but also some bi-directional  
211 flows in the sheath. A clear sustained drop in plasma density, the onset of sustained  
212 bi-directional suprathermal electrons, and the start of smooth magnetic field rotations  
213 indicate the arrival of the ME portion of the ICME at 22:00:57 UT on 1 January 2012.

214 The ME portion of the ICME (between the second and third magenta lines, and shown  
215 in higher resolution in Figure 4), which lasted from 22:00:57 UT on 1 January 2012 until  
216 18:57:45 on 2 January 2012, exhibits a smooth rotation in the magnetic field direction and  
217 low variability magnetic field in general, with  $B_R$  and  $B_T$  being the dominant magnetic  
218 field components. However, near the center of the ME crossing, a region with different  
219 properties compared with the rest of the ME was encountered on January 2nd at 04:00:00  
220 and lasted until 10:21:26 UT (marked by black vertical lines in Figure 3). This turbulent  
221 region is characterized by high magnetic field fluctuations, high plasma density, an increase  
222 in velocity, fluctuating temperature, and a small increase in the average iron charge state.  
223 The increase in average iron charge state implies a different source for the plasma in this  
224 region than for the rest of the ME, while the overall increased value of plasma  $\beta$  in the  
225 region strongly implies plasma heating. We have also tested that this turbulent region  
226 is not a planar structure. Plasma velocity measurements show a change in polarity in  
227 the tangential component of the velocity vector,  $v_T$  (not shown here), just at the start

228 of the turbulent region. A change in sign of the azimuthal flow angle, for which  $v_T$  is  
229 a proxy, indicates a stream interface [Gosling & Pizzo, 1999]. The measurements also  
230 indicate that there is likely a slow mode shock near 06:00 UT due to the sharp increase in  
231 density, temperature and velocity, along with a corresponding sharp decrease in magnetic  
232 field magnitude. The combination of these data in this distinct region hints at signatures  
233 of reconnection, which likely occurred between the flux rope and the HPS/HCS that the  
234 ICME overtook during propagation (see Section 4).

235 The strongest case for signatures of reconnection in this region, however, is made by  
236 the suprathermal electrons. Within the ME, both before and after the turbulent region,  
237 STEREO A measured counter-streaming electrons, while within the region, the pitch angle  
238 distribution was highly variable. There are clear intervals when bi-directional flows are  
239 detected but they are interspersed with sharp drop-outs to uni-directional flows only. This  
240 alternating signature of short bursts of bi-directional then uni-directional flows implies the  
241 succession of closed to open field lines (i.e., both ends connected at the Sun or only one  
242 end connected), indicating interchange reconnection. We discuss the implications of these  
243 signatures further in Section 4 and 5 of the paper.

244 It is also worth mentioning, that even though a return to the smooth rotation in the  
245 magnetic field direction, low plasma density, and decrease in plasma velocity and plasma  $\beta$   
246 indicate the return to the non-turbulent part of the ME at  $\sim 10:20$  UT, sustained counter-  
247 streaming suprathermal electrons only return  $\sim 4$  hours later, marked by the dashed verti-  
248 cal line in Figures 3 and 4. STEREO A then spent another  $\sim 8.5$  hours in the ME, which  
249 displayed similar properties to those observed prior to the encounter of the turbulent re-  
250 gion. The end of the ME passage (last magenta vertical guideline) was identified based

251 on the start of large magnetic field fluctuations and the end of the steady magnetic field  
252 magnitude decrease. However, since there are no clear indicators in the plasma data, the  
253 ICME end time carries some uncertainty.

254 Due to the interruption of the ME by the turbulent region, the question whether there  
255 are actually two distinct flux ropes from two separate ICMEs, naturally arises. This  
256 hypothesis, although plausible at first sight, fails to explain several measurements. First,  
257 MESSENGER only observes one flux rope at Mercury. Second, if separated, the duration  
258 of each flux rope (excluding the turbulent region) at STEREO A ( $\sim 6$  hours and  $\sim 8$  hours)  
259 is much shorter than the flux rope duration observed at Mercury ( $\sim 12$  hours), which is  
260 contrary to the expectation that ICMEs expand as they propagate outwards in the solar  
261 system. Lastly, if separated, neither flux rope would actually meet the definition of a flux  
262 rope given that neither on its own exhibits a smooth rotation in  $\mathbf{B}$ . Thus, our initial  
263 scenario, that there is only one flux rope, which underwent reconnection with corotating  
264 disturbances in the solar wind, is the most likely scenario.

### 3. Force-free field fitting and ICME speed

265 Initial comparison between the large-scale magnetic field structure in the ME at MES-  
266 SENER and at STEREO A shows that rotation in the magnetic field occurred during  
267 propagation. To quantify the change in the magnetic field direction, we determined the  
268 flux rope orientation at the two spacecraft by conducting force-free field fits to the data.  
269 Here the model used is a non-expanding, constant  $\alpha$  force-free field model as developed  
270 by Burlaga [1988] and we used a  $\chi^2$  minimization procedure as optimized by Lepping et  
271 al. [1990]. The flux rope axis orientation is first evaluated via minimum variance analysis,  
272 which is then used as the starting point for the force-free field fits. For the fits at 1 AU,

273 we did not include data during the highly turbulent interval in the ME between 04:06:45  
274 and 10:20:50 UT.

275 The force-free field fits (Figure 5) yield a left-handed flux rope at both spacecraft,  
276 with  $\theta = -12.3^\circ \pm 0.4^\circ$ ,  $\phi = 131^\circ \pm 1^\circ$ , and  $B_0 = 55.9 \pm 0.5$  nT at MESSENGER, and  
277  $\theta = 66^\circ \pm 1^\circ$ ,  $\phi = 197^\circ \pm 8^\circ$ , and  $B_0 = 12.3 \pm 0.5$  nT at STEREO A, where the uncertainties  
278 represent 3-sigma statistical errors. Here  $\theta$  is the angle between the flux rope axis and  
279 the ecliptic plane,  $\phi$  is the angle from the anti-sunward direction anticlockwise to the  
280 projection of the axis direction onto the ecliptic plane, and  $B_0$  is the field strength along  
281 the flux rope axis.

282 The  $\sim 80^\circ$  difference in latitude and  $\sim 65^\circ$  difference in longitude of the flux rope axis  
283 between MESSENGER and STEREO A imply a significant rotation of the flux rope during  
284 propagation. We discuss in detail the likely causes of this rotation in the next section.  
285 Although we use one of the simplest models for the magnetic field reconstruction, we  
286 consider the result that the flux rope orientation changed between MESSENGER and  
287 STEREO A to be very robust. This is because the dominant component of the magnetic  
288 field and the sense of rotation of the  $B_T$  and  $B_N$  components differ at MESSENGER and  
289 STEREO A, as shown in Figures 2 and 3.

290 The force-free fitting also yielded  $B_0 \propto r^{-1.83}$  where  $r$  is heliocentric distance, in good  
291 agreement with results obtained from the statistical study on all the ICMEs observed at  
292 MESSENGER by Winslow et al. [2015] and with other past studies using Helios data  
293 [e.g., Gulisano et al., 2010]. The factor of  $\sim 5$  decrease in the flux rope axial field strength  
294 is a clear indication of expansion of the cloud as it propagates from Mercury to 1 AU. An  
295 impact parameter of  $\sim 0.5$  was obtained at both spacecraft, where the impact parameter

296 is defined as the distance of closest approach of the spacecraft to the flux rope axis  
297 normalized by the radius of the flux rope. It is also worth mentioning that the fits had  
298 low  $\chi^2$  values of 0.09 at MESSENGER and 0.06 at STEREO A, indicating good quality  
299 fits at both spacecraft.

300 From the time of the CME launch at the Sun, the Sun-Mercury distance, and the arrival  
301 time at Mercury we can determine the average ICME speed between the Sun and Mercury.  
302 We can similarly obtain an average ICME speed between Mercury and STEREO A. Our  
303 results indicate an average shock speed from the Sun to Mercury of  $\sim 710 \text{ km s}^{-1}$ , while  
304 from Mercury to STEREO A we find an average shock transit speed of  $\sim 500 \text{ km s}^{-1}$ . At  
305 STEREO A this yields a  $\sim 50 \text{ km s}^{-1}$  overestimate of the ICME shock speed, as Figure 3  
306 shows the in situ measured speed to be  $\sim 450 \text{ km s}^{-1}$ .

307 We can also estimate the ICME speed from the drag-based model [Vršnak et al., 2013]  
308 available online at <http://oh.geof.unizg.hr/DBM/dbm.php>. The drag-based model as-  
309 sumes that after initial CME acceleration, aerodynamic drag is the dominant force acting  
310 on the CME. We used the following parameter values for the drag-based model: CME  
311 take-off date and time 12/29/2011 21:11:00 at  $20 R_{Sun}$ , initial CME speed of  $750 \text{ km s}^{-1}$ ,  
312 solar wind speed of  $350 \text{ km s}^{-1}$ , and  $\gamma$ , the drag parameter, of  $0.1 \times 10^{-7}$ . At Mercury, at  
313  $0.42 \text{ AU}$ , the model yields an ICME arrival time at 12/30/2011 16:29:00 with a speed of  
314  $663 \text{ km s}^{-1}$ , which matches the MESSENGER observed arrival time perfectly. Interest-  
315 ingly, if we assume the same drag parameter value throughout propagation all the way to  
316  $1 \text{ AU}$ , we find an arrival time of 01/01/2012 08:03:00 with a speed of  $566 \text{ km s}^{-1}$  at  $1 \text{ AU}$ .  
317 This yields a 5 hours earlier arrival time than what was actually observed, and the speed  
318 is about  $100 \text{ km s}^{-1}$  faster than what is observed by STEREO A. This suggests that likely

319 due to the ICME interacting with corotating structures in the Mercury-to-STEREO A  
320 transit space, it may not be appropriate to use the same drag parameter for the entire  
321 propagation distance. If we use a drag parameter value of  $0.18 \times 10^{-7}$  for estimating the  
322 ICME arrival to 1 AU, we find an arrival time of 13:31:00 with a speed of  $500 \text{ km s}^{-1}$  at  
323 STEREO A. This is only  $\sim 10$  mins off the arrival time and  $50 \text{ km s}^{-1}$  off the measured  
324 speed. Additionally, this scenario implies an ICME speed of  $612 \text{ km s}^{-1}$  at MESSENGER,  
325 which together with the previous scenario yields an upper and lower bound for the ICME  
326 speed at MESSENGER of  $640 \pm 25 \text{ km s}^{-1}$ . Taking the ICME speed at Mercury to be  
327  $640 \text{ km s}^{-1}$  from the drag-based model and the ICME speed to be  $450 \text{ km/s}$  as measured  
328 at 1 AU, we find a speed decrease of  $\sim 30\%$ , suggesting a significant speed decrease from  
329 Mercury to 1 AU, in line with our statistical study presented in Winslow et al. [2015].

#### 4. Background solar wind conditions

330 The significant change observed in the flux rope orientation implies strong interaction  
331 with the solar wind. In this Section, we discuss both the measurements and simulations  
332 of the background solar wind in which the ICME propagated from MESSENGER to  
333 STEREO A. First, through simple inspection of the magnetic field measurements we can  
334 piece together a likely scenario. Magnetic field data at MESSENGER and STEREO  
335 A show that prior to the ICME shock arrival, the IMF  $B_R$  component was positive at  
336 Mercury and negative at STEREO A (see Figures 2 and 3). This is evidence for the ICME  
337 having encountered the heliospheric current sheet during propagation between Mercury  
338 and 1 AU. Furthermore, the magnetic field data alone yield insight as to when this might  
339 have happened. We can see that after the ICME passage, STEREO A re-emerges into the  
340 interplanetary medium where the IMF  $B_R$  component is positive. Thus just before the



341 ICME arrived at STEREO A the spacecraft was in a negative polarity IMF, while just  
342 after the ICME passage the spacecraft was in a positive polarity IMF.

343 Further detail can be glimpsed from Figure 6, which shows STEREO A data a few  
344 days before and after (including) the ICME. Vertical lines demarcate the boundaries of  
345 the ICME (as described in Section 2). Prior to the ICME shock arrival, there is a steep  
346 decrease in  $|B|$ , increase in density, increase in  $\beta$ , as well as a slow decrease in velocity  
347 starting at  $\sim 03:00$  UT on 1 January 2012. During the same time, the suprathermal  
348 electrons exhibit a change first from somewhat bi-directional to mostly uni-directional  
349 flow opposite to the strahl, and then back again to a strong strahl component. We also  
350 note that the iron charge state distribution shows a change from an average value of 10  
351 to an average value of 12 near 03:00 UT on January 1st (see Figure 3). An important  
352 property of ionic charge states is that they remain virtually constant after the freeze-in  
353 point ( $\sim 10 R_S$ ), and thus they represent different sources for the plasma close to the  
354 Sun. We attribute all of these changes to the vicinity of an extended heliospheric plasma  
355 sheet (in which the HCS is embedded). All these changes come at the tail end of a high  
356 speed stream following a corotating interaction region (CIR) on 28 December 2011. The  
357 combination of signatures observed at the time before the ICME arrival, specifically the  
358 very low  $|B|$  ( $< 1$  nT), increase in density and in  $\beta$ , suggest that the spacecraft encountered  
359 the HPS. This is further supported by the change in sign of  $B_R$  and the clear change in  
360 the suprathermal electron strahl direction from  $180^\circ$  to  $0^\circ$  during the ICME passage.  
361 These observations are directly in line with those by Winterhalter et al. [1994] of the  
362 HPS, which show that on average, the HCS is displaced from the center of the HPS in

363 which it is embedded, as is the case here. Thus the measurements suggest that the ICME  
364 encountered and overtook the HCS and part of the HPS before reaching STEREO A.

365 The linearly decreasing speed profile on January 1, has raised the possibility that this  
366 feature might be a small ICME as opposed to the HPS, with the measured low magnetic  
367 field magnitude being due to over-expansion. This is unlikely, given the near-zero magnetic  
368 field value, the increase in plasma density, and the increased plasma  $\beta$ . We have also  
369 checked for possible CME candidates that could have resulted in an ICME prior to the 29  
370 December ICME, with only two meeting the direction criteria. As these two CMEs (both  
371 launched on 27 December) are much smaller and fainter than the 29 December CME and,  
372 as they originate from  $15^\circ$ - $20^\circ$  from disk center, they are unlikely to have resulted in strong  
373 and/or long-lasting disturbances in the solar wind at 1 AU as measured by STEREO A.

374 Steady state solar wind simulation results from the ENLIL model [Odstrcil, 2003] are  
375 shown in Figure 7a-b for two different times: just after the ICME reached Mercury and  
376 just before the ICME reached STEREO A. The simulations were run at the Community  
377 Coordinated Modeling Center for Carrington Rotation 2118, with the MAS coronal model  
378 [Linker et al., 1999; Mikic et al., 1999] and magnetogram data obtained from the Kitt Peak  
379 observatory. Both figures show normalized solar wind density in the ecliptic plane as a  
380 function of longitude. The IMF polarity is indicated as red (positive) or blue (negative)  
381 coloring of the circular border, and we note that the HCS is marked by the white line in the  
382 figures. The simulation results clearly show an HCS between Mercury and STEREO A,  
383 confirming the scenario gleaned from magnetic field data. They indicate the HCS having  
384 passed by Mercury prior to the ICME arrival, while at STEREO A, the HCS arrives just  
385 after the ICME. The simulations also reveal that the HCS is embedded in the HPS, as

386 seen by the region of high density plasma following the HCS in Figure 7a-b. Based on  
387 these data and the simulations, we have a clearer picture of the sequence of events which  
388 transformed a relatively straightforward ICME and flux rope at MESSENGER into a  
389 highly disturbed one at STEREO A:

390 1. The ICME is ejected into positive polarity IMF and relatively undisturbed solar  
391 wind.

392 2. At Mercury, the passage of the HPS/HSC is observed in the magnetic field data at  
393  $\sim 5:00$  UT on 29 December 2011,  $\sim 1.5$  days prior to the ICME arrival, so the ICME does  
394 not interact with it yet. Therefore, MESSENGER observes a fairly undisturbed ICME  
395 with a straightforward flux rope that has a latitudinal orientation close (within  $\sim 20^\circ$ ) to  
396 that expected from the GCS model of the CME soon after launch.

397 3. During propagation from Mercury to STEREO A, the ICME catches up to part of  
398 the HPS. It is likely that the turbulent region observed within the flux rope at STEREO A  
399 is highly compressed plasma from the HPS that was engulfed by the ICME. This complex  
400 structure at 1 AU (especially in light of the suprathermal electron data), compared with  
401 the measurements at MESSENGER, suggests that extensive magnetic reconnection took  
402 place between the ICME and the HPS/HCS magnetic fields. The ICME likely overtook  
403 the HCS just prior to reaching STEREO A. The complexity in the ICME composition at  
404 STEREO A that arose due to the ICME interacting with the HPS and HCS is further  
405 evidenced by the iron charge state data.

406 Similarly, in a recent paper, [Prise et al. \[2015\]](#) observe an ICME overtaking and merging  
407 with a CIR, although in their case this occurs further out in the solar system, between  
408 Mars' and Saturn's orbits. For our event, the observations and simulations paint the

409 picture of an ICME with a fairly simple initial structure that was made significantly more  
410 complex due to interaction with existing disturbances in the solar wind. Our example  
411 provides direct evidence for solar wind induced alteration of the magnetic topology within  
412 ICMEs.

## 5. Discussion and Conclusions

413 In this paper we present a case study of the evolution of a CME ejected from the Sun  
414 on 29 December 2011 as it propagates from the Sun to Mercury and then to 1 AU. At  
415 MESSENGER, magnetic field measurements present a fairly simple ICME structure with  
416 ordered magnetic fields indicative of a MC. Despite the near-perfect longitudinal align-  
417 ment between MESSENGER and STEREO A during the time the CME propagates from  
418 Mercury to 1 AU, STEREO A data indicate a significantly altered and more disturbed  
419 ICME.

420 The three most striking features of this ICME are: 1) the significantly changed mag-  
421 netic topology between MESSENGER and STEREO A (seen both in the magnetic field  
422 measurements and from the flux rope fitting); 2) the enclosed turbulent region within the  
423 center of the ICME observed at STEREO A but not at MESSENGER; and 3) the clear  
424 variation at STEREO A from counter-streaming to uni-directional suprathermal electron  
425 flows in the turbulent region, implying variation between closed and open magnetic field  
426 lines as the spacecraft travels through this reconnection region. These features illustrate  
427 the increased complexity in ICME structure during propagation from 0.42 AU at MES-  
428 SENGER to 0.96 AU at STEREO A due to strong interaction of the ICME with the solar  
429 wind.

430 Significant alteration of the magnetic topology requires reconnection to occur either  
431 within the ICME or between the ICME and the IMF. Gosling et al. [1995] first discussed  
432 how sustained 3-dimensional reconnection close to the Sun between different sheared or  
433 skewed coronal loops can alter the flux rope topology and produce field lines within CMEs  
434 that are open and/or are connected to the outer heliosphere at both ends. Their Figure  
435 6 exemplifies several different magnetic topologies that can arise in CMEs that have  
436 undergone 3-dimensional reconnection. In addition, based on observational evidence and  
437 theoretical considerations, Fermo et al. [2014] showed that any deviation from the lowest  
438 energy state of a flux rope, the so-called Taylor state, will result in reconnection occurring  
439 within the interior of the flux rope.

440 The ICME event presented in this paper likely has undergone 3-dimensional reconnection,  
441 specifically interchange reconnection [e.g., Lugaz et al., 2011; Masson et al., 2013],  
442 and thus the reconnection did not occur within the ICME itself but with the magnetic  
443 fields of the HPS/HCS in the solar wind. The short duration, multiple successions of  
444 bi-directional and uni-directional suprathermal electron flows in the turbulent region are  
445 indicative of the spacecraft traversing a succession of closed and open field lines within  
446 this short time frame. We infer that most likely the closed field lines of the ICME, interchange  
447 reconnected with the open field lines of the HPS in transit between  $\sim 0.4$  and  $\sim 1$   
448 AU, thereby opening up some of the closed ICME field lines. Figure 8 shows a simplified  
449 cartoon example of the possible reconnection scenario between the flux rope and the HPS  
450 field line. It has been shown both through observations [e.g., Dasso et al., 2006, 2007;  
451 Möstl et al., 2008; Ruffenach et al., 2012] and MHD simulations [e.g., Schmidt & Cargill,  
452 2003; Taubenschuss et al., 2010] that reconnection between the front of a magnetic cloud

453 and the IMF alters the flux rope topology and causes erosion of the ICME. Through a  
454 large statistical study, Ruffenach et al. [2015] showed that MCs can be eroded at both the  
455 front and rear ends in similar proportions, i.e., reconnection between the flux rope and  
456 the IMF can occur at the front or the rear of the ICME.

457 The event discussed in this paper, however, seems to differ from these scenarios in that  
458 the reconnected region between the HPS and ICME lies at the center of the ME as opposed  
459 to the front or the rear. A possible explanation is that due to reconnection between the  
460 front of the ICME and the HPS magnetic field, not only did the overall magnetic topology  
461 of the flux rope change, but part of the wind stream within the HPS became enveloped  
462 by the expanding ME. The turbulent region observed within the flux rope at STEREO A  
463 appears to be an inclusion of HPS plasma. A possible way that this could have occurred is  
464 that the ICME “engulfed” the HPS by expanding around it in latitude. Due to the higher  
465 density of the HPS in the ecliptic, the front central part of the ICME likely interacted with  
466 the HPS, which is where the reconnection occurred, but the flanks of the ICME may have  
467 been deflected around the HPS in latitude and later expanded back to the ecliptic. This  
468 scenario could explain the relative central appearance of the reconnected region within  
469 the flux rope, and the large change in overall flux rope orientation. We note that it is  
470 possible, that to some extent the relative central appearance of the turbulent region within  
471 the ME is caused by a limitation in the observations due to the large-scale 3-dimensional  
472 nature of the ICME compared to the 1-dimensional nature of the spacecraft crossing.  
473 However, some amount of envelopment of HPS plasma by the ME is required by the  
474 measurements regardless of the crossing geometry. Further modeling work is necessary to

475 test whether the expansion of the ME, especially in latitude, can account for the relative  
476 central appearance of the reconnection region within the flux rope.

477 The idea that complexity in ICME structure increases with heliocentric distance due to  
478 prolonged interaction with the solar wind has been studied in the past. For example, the  
479 fact that the MC fraction at 1 AU displays a strong solar cycle dependence [Richardson  
480 & Cane, 2010], with the highest MC fraction observed at solar minimum when the Sun is  
481 most quiet, is an indication that the MC fraction does reflect to some extent interaction  
482 between ICMEs and other solar transients in the solar wind during transit [Richardson &  
483 Cane, 2004]. Thus the relative decrease in MC fraction with heliocentric distance can be  
484 used as a proxy measure of increasing complexity in ICMEs.

485 Analyzing a small subset of inner heliospheric observations by the Helios spacecraft  
486 between 1979 and 1981, Bothmer & Schwenn [1996] found that 7 out of 17 (41%) ICMEs  
487 exhibited MC characteristics. Indirect evidence suggests that a large fraction of the 61  
488 ICMEs cataloged by Winslow et al. [2015] between 2011 and 2014 at Mercury's orbit  
489 are MCs, although an exact number cannot be determined due to the lack of solar wind  
490 plasma observations with MESSENGER. At 1 AU, over the solar cycle, approximately  
491 one-third of ICMEs show MC signatures [Gosling, 1990; Richardson & Cane, 2010]. Be-  
492 yond Earth's orbit, Rodriguez et al. [2004] using Ulysses observations between 1 and 5  
493 AU found 40 out of 148 (27%) ICMEs to be MCs. Overall, this is a modest drop in MC  
494 fraction from 0.3 to 5 AU and a slight indication of increased complexity, incorporating  
495 studies of varying statistical significance and during different solar cycles. Studying the  
496 evolution of complexity in ICMEs with heliocentric distance requires multipoint in situ  
497 magnetic field and or plasma data, making such studies difficult to attain in the past due

498 to lack of adequate measurements. The recently completed MESSENGER mission and  
499 the upcoming Solar Probe Plus and Solar Orbiter missions to the innermost heliosphere  
500 in the next few years should help in this regard. Our paper provides a concrete example of  
501 increased complexity in ICME structure from Mercury to 1 AU solely due to interaction  
502 of the ICME with an HCS and HPS in the solar wind.

503 This increase in complexity and large change in magnetic topology during propagation  
504 has not only significant implications for ICME evolution in the solar wind but also for  
505 geomagnetic storm forecasting. The magnetic field direction and duration in the ICME  
506 largely determines the likelihood of geomagnetic storm onset. Our results show that  
507 depending on the timing of ICME eruptions and the presence of corotating structures  
508 in the solar wind, magnetic field measurements in the innermost heliosphere may not be  
509 accurate in predicting ICME magnetic field direction at the Earth. However, the timing  
510 and location of HPS' and HCS' can be modeled fairly accurately due their corotating  
511 nature [Jian et al., 2015]. Thus geomagnetic storm forecasting based on in situ magnetic  
512 field data upstream of the Earth may still be accurate at times when corotating structures  
513 are not present in the ICME transit path from the Sun to 1 AU. These results also highlight  
514 the need for a statistical study to evaluate the frequency of significant alterations in flux  
515 rope orientation during propagation between the innermost heliosphere and 1 AU.

516 **Acknowledgments.** Support for this work was provided by the NASA Lunar  
517 Reconnaissance Orbiter Project (NASA contract NNG11PA03C), as well as various  
518 NASA grants (EMMREM, grant NNX07AC14G; C-SWEPA, grant NNX07AC14G;  
519 DoSEN, grant NNX13AC89G; DREAM, grant NNX10AB17A; and DREAM2; grant  
520 NNX14AG13A) and a NSF grant (Sun-2-Ice, grant AGS1135432). We also thank the



521 International Space Science Institute for supporting the Research Team: Radiation  
522 Interactions at Planetary Bodies (<http://www.issibern.ch/teams/interactplanetbody/>).

523 N. L. acknowledges support from NASA grant NNX15AB87G and NNX13AP52G. We  
524 also acknowledge support from the STEREO-FARSIDE grant (NNX13AP52G) to the  
525 University of New Hampshire. MESSENGER data are available on the Planetary  
526 Data System (<https://pds.jpl.nasa.gov>). STEREO data are available on the Space  
527 Physics Data Facility (<http://cdaweb.gsfc.nasa.gov>). Simulation results (run number  
528 Reka\_Winslow\_110515\_SH\_1) have been provided by special request from the Commu-  
529 nity Coordinated Modeling Center at Goddard Space Flight Center through their public  
530 Runs on Request system (<http://ccmc.gsfc.nasa.gov>). The MAS model was developed by  
531 J. Linker, Z. Mikic, R. Lionello, and P. Riley and the ENLIL Model was developed by D.  
532 Odstrcil. We thank two anonymous reviewers for their comments on the paper.

## References

- 533 Andrews, G. D. et al. 2007, The Energetic Particle and Plasma Spectrometer instrument  
534 on the MESSENGER spacecraft, *Space Science Reviews*, 131, 523
- 535 Bothmer, V. and R. Schwenn (1996), Signatures of fast CMEs in interplanetary space,  
536 *Adv. Space Res.*, 17, 319-322.
- 537 Burlaga, L.F. (1988), Magnetic clouds and force-free fields with constant alpha, *J. Geo-*  
538 *phys. Res.*, 93, 7217. doi:10.1029/JA093iA07p07217.
- 539 Cane, H. V., & I. G. Richardson 2003, Interplanetary coronal mass ejections in the near-  
540 Earth solar wind during 1996-2002, *Journal of Geophysical Research (Space Physics)*,  
541 108, 1156.

- 542 Dasso, S., C. H. Mandrini, P. Demoulin, and M. L. Luoni (2006), A new model-  
543 independent method to compute magnetic helicity in magnetic clouds, *Astron. Astro-*  
544 *phys.*, 455, 349-359, doi:10.1051/0004-6361: 20064806.
- 545 Dasso, S., M. S. Nakwacki, P. Demoulin, and C. H. Mandrini (2007), Progressive trans-  
546 formation of a flux rope to an ICME, *Sol. Phys.*, 244, 115-137, doi:10.1007/s11207-007-  
547 9034-2.
- 548 Farrugia, C. J., I. G. Richardson, L. F. Burlaga, R. P. Lepping, and V. A. Osherovich  
549 (1993), Simultaneous observations of solar MeV particles in a magnetic cloud and in  
550 the Earth's northern tail lobe: Implications for the global field line topology of magnetic  
551 clouds and for the entry of solar particles into the magnetosphere during cloud passage,  
552 *J. Geophys. Res.*, 98, 15,497-15,507.
- 553 Farrugia, C. J., L.F. Burlaga, and R. P. Lepping (1997), Magnetic Clouds and the  
554 quiet/storm effect at Earth: A review, in *Magnetic Storms*, Geophysical Monogr. Ser.,  
555 vol. 98, pp. 91, edited by B. T. Tsurutani, W. D. Gonzalez, Y. Kamide, and J. K.  
556 Arballo, AGU, Washington, D. C.
- 557 Fermo, R. L., M. Opher, and J. F. Drake (2014), Magnetic reconnection in the  
558 interior of interplanetary coronal mass ejections, *Phys. Rev. Lett.*, 113, 031101,  
559 doi:10.1103/PhysRevLett.113.031101.
- 560 Fox, N. J. et al. (2015), The Solar Probe Plus mission: Humanity's first visit to our star,  
561 *Space Sci. Rev.*, doi:10.1007/s11214-015-0211-6.
- 562 Galvin, A. B. et al. (2008), The Plasma and Suprathermal Ion Composition (PLAS-  
563 TIC) investigation on the STEREO observatories, *Space Sci. Rev.*, 136, 437-486,  
564 doi:10.1007/s11214-007-9296-x.

- 565 Gershman, D. J. et al. 2012, Solar wind alpha particles and heavy ions in the inner helio-  
566 sphere observed with MESSENGER, *Journal of Geophysical Research (Space Physics)*,  
567 117, A00M02
- 568 Good, S. W., R. J. Forsyth, J. M. Raines, D. J. Gershman, J. A. Slavin, and T. H.  
569 Zurbuchen (2015), Radial evolution of a magnetic cloud: MESSENGER, STEREO,  
570 and Venus Express observations, *ApJ*, 807, 177, doi:10.1088/0004-637X/807/2/177.
- 571 Gonzalez, W. D. and B. T. Tsurutani (1987), Criteria of interplanetary parameters causing  
572 intense magnetic storms ( $D < -100$  nT), *Planet. Space Sci.*, 35, 1101.
- 573 Gosling, J. T. (1990), Coronal Mass Ejections and Magnetic Flux Ropes in Interplanetary  
574 Space, in *Physics of Magnetic Flux Ropes*, ed. by E.R. Priest, L.C. Lee, C.T. Russell,  
575 AGU Geophys. Monogr. 58, 343-364.
- 576 Gosling, J. T., J. Birn, and M. Hesse (1995), Three-dimensional magnetic reconnection  
577 and the magnetic topology of coronal mass ejection events, *Geophys. Res. Lett.*, 22,  
578 869-872.
- 579 Gosling, J. T. & V. J. Pizzo (1999), Formation and evolution of corotating interaction  
580 regions and their three dimensional structure, *Space Sci. Rev.*, 89, 21-52.
- 581 Gulisano, A. M., P. Demoulin, S. Dasso, M. E. Ruiz, and E. Marsch (2010), Global and  
582 local expansion of magnetic clouds in the inner heliosphere, *Astron. Astrophys.*, 509,  
583 A39.
- 584 Jian, L., C. T. Russell, J. G. Luhmann, and R. M. Skoug (2006), Properties of stream  
585 interactions at one AU during 19952004, *Sol. Phys.*, 239, 337392, doi:10.1007/s11207-  
586 006-0132-8

- 587 Jian, L. K., P. J. MacNeice, A. Taktakishvili, D. Odstrcil, B. Jackson, H.-S. Yu, P.  
588 Riley, I. V. Sokolov, R. M. Evans (2015), Validation for solar wind prediction at Earth:  
589 Comparison of coronal and heliospheric models installed at the CCMC, Space Weather,  
590 13, 316-338, doi:10.1002/2015SW001174.
- 591 Kay, C., Opher, M., & Evans, R. M. 2013, Forecasting a Coronal Mass Ejection's Altered  
592 Trajectory: ForeCAT, The Astrophysical Journal, 775, 5.
- 593 Kay, C., Opher, M., & Evans, R. M. 2015, Global Trends of CME Deflections Based on  
594 CME and Solar Parameters, The Astrophysical Journal, 805, 168.
- 595 Kliem, B., Török, T., & Thompson, W. T. 2012, A Parametric Study of Erupting Flux  
596 Rope Rotation. Modeling the "Cartwheel CME" on 9 April 2008, Solar Physics, 281,  
597 137.
- 598 Kubicka, M., C. Möstl, P. D. Boakes, L. Feng, J. P. Eastwood, O. Törmänen (2016),  
599 Prediction of geomagnetic storm strength from inner heliospheric in situ observations,  
600 J. Geophys. Res.,
- 601 Lavraud, B., Puffenach, A., Rouillard, A. P., et al. 2014, Geo-effectiveness and radial  
602 dependence of magnetic cloud erosion by magnetic reconnection, Journal of Geophysical  
603 Research (Space Physics), 119, 26.
- 604 Lepping, R.P., L. F. Burlaga, J. A. Jones (1990), Magnetic field structure of interplanetary  
605 magnetic clouds at 1 AU, J. Geophys. Res. 95, 11957.
- 606 Lindsay, C. M., C. T. Russell, and J. G. Luhmann (1995), Coronal mass ejection and  
607 stream interaction region characteristics and their potential geomagnetic effectiveness,  
608 J. Geophys. Res., 100, 16,999-17,013.

- 609 Linker, J., et al. (1999), Magnetohydrodynamic modeling of the solar corona during whole  
610 sun month, *J. Geophys. Res.*, 104, 9809 - 9830.
- 611 Luhmann, J. G. et al. (2008), STEREO IMPACT investigation goals, measurements, and  
612 data products overview, *Space Sci. Rev.*, 136, 117-184, doi:10.1007/s11214-007-9170-x.
- 613 Lugaz, N. C., Downs, K., Shibata, I. I., Roussev, A., Asai, and T. I. Gombosi (2011),  
614 Numerical investigation of a coronal mass ejection from an anemone active region:  
615 reconnection and deflection of the 2005 August 22 eruption, *The Astrophysical Journal*,  
616 738, 127, doi:10.1088/0004-637X/738/2/127.
- 617 Lynch, B. J., T. H. Zurbuchen, L. A. Fisk, and S. K. Antiochos (2003), Internal  
618 structure of magnetic clouds: Plasma and composition, *J. Geophys. Res.*, 108, 1239,  
619 doi:10.1029/2002JA009591.
- 620 Lynch, B. J., Antiochos, S. K., Li, Y., Luhmann, J. G., & DeVore, C. R. 2009, Rotation  
621 of Coronal Mass Ejections during Eruption, *The Astrophysical Journal*, 697, 1918.
- 622 Maloney, S. A., P. T. Gallagher & R. T. J. McAteer 2009, Reconstructing the 3-D trajec-  
623 tories of CMEs in the inner heliosphere, *Solar Physics*, 256, 149
- 624 Manchester, W. B. IV et al. (2004), Modeling a space weather event from the Sun to  
625 the Earth. CME generation and interplanetary propagation, *Journal of Geophysical  
626 Research (Space Physics)*, 109, A02107
- 627 Manchester, W. B. IV et al. (2005), Coronal mass ejection shock and sheath structures  
628 relevant to particle acceleration, *The Astrophysical Journal*, 622, 1225-1239.
- 629 Masson, S., S. K. Antiochos, and C. R. DeVore (2013), A model for the escape of  
630 solar-flare accelerated particles, *The Astrophysical Journal*, 771, 82, doi:10.1088/0004-  
631 637X/771/2/82.

- 632 Mikic, Z., J. A. Linker, D. D. Schnack, R. Lionello, and A. Tarditi (1999), Magneto-  
633 hydrodynamic modeling of the global solar corona, *Phys. Plasma*, 6, 2217- 2224.
- 634 Möstl, C., C. Miklenic, C. J. Farrugia, M. Temmer, A. Veronig, A. B. Galvin, and H. K.  
635 Biernat (2008), Two-spacecraft reconstruction of a magnetic cloud and comparison to  
636 its solar source, *Ann. Geophys.*, 26, 3139-3152, doi:10.5194/angeo-26-3139-2008.
- 637 Möstl, C. et al. 2012, Multi-point shock and flux rope analysis of multiple interplanetary  
638 coronal mass ejections around 2010 August 1 in the inner heliosphere, *The Astrophysical*  
639 *Journal*, 758, 10
- 640 Müller, D., & O. C. St. Cyr 2013, The Solar Orbiter mission, *Proceedings of the SPIE*,  
641 8862, 88620E
- 642 Nieves-Chinchilla, T., R. Colaninno, A. Vourlidas, A. Szabo, R. P. Lepping, S. A. Board-  
643 sen, B. J. Anderson, and H. Korth (2012), Remote and in situ observations of an unusual  
644 Earth-directed coronal mass ejection from multiple viewpoints, *J. Geophys. Res.*, 117,  
645 A06106, doi:10.1029/2011JA017243.
- 646 Odstrcil, D. 2003, Modeling 3-D solar wind structure, *Advances in Space Research*, 32,  
647 497.
- 648 Palmerio, E., E. K. J. Kilpua, N. P. Savani (2016), Planar magnetic structures in coronal  
649 mass ejection-driven sheath regions, *Ann. Geophys.*, 34, 313-322.
- 650 Prise, A. J., L. K. Harra, S. A. Matthews, C. S. Arridge, and N. Achilleos (2015), Analysis  
651 of a coronal mass ejection and corotating interaction region as they travel from the Sun  
652 passing Venus, Earth, Mars, and Saturn, *J. Geophys. Res. Space Physics*, 120, 15661588,  
653 doi:10.1002/2014JA020256.

- 654 Richardson, I. G., and H. V. Cane (2004), The fraction of interplanetary coronal mass  
655 ejections that are magnetic clouds: Evidence for a solar cycle variation, *Geophys. Res.*  
656 *Lett.*, 31, L18804, doi:10.1029/2004GL020958.
- 657 Richardson, I. G., & H. V. Cane 2010, Near-Earth interplanetary coronal mass ejections  
658 during solar cycle 23 (19962009): Catalog and summary of properties, *Solar Physics*,  
659 264, 189.
- 660 Rodriguez, L., J. Woch, N. Krupp, M. Fränz, R. von Steiger, R. J. Forsyth, D. B. Reisen-  
661 feld, and K. H. Glassmeier (2004), A statistical study of oxygen freezing-in temperature  
662 and energetic particles inside magnetic clouds observed by Ulysses, *J. Geophys. Res.*,  
663 109, A01108, doi:10.1029/2003JA010156.
- 664 Ruffenach, A. et al. (2012), Multispacecraft observation of magnetic cloud erosion  
665 by magnetic reconnection during propagation, *J. Geophys. Res.*, 117, A09101,  
666 doi:10.1029/2012JA017624.
- 667 Ruffenach, A., Lavraud, B., Farrugia, C. J., et al. 2015, Statistical study of magnetic cloud  
668 erosion by magnetic reconnection, *Journal of Geophysical Research (Space Physics)*,  
669 120, 43.
- 670 Rouillard, A. P., et al. (2009), A solar storm observed from the Sun to Venus using  
671 the STEREO, Venus Express, and MESSENGER spacecraft, *J. Geophys. Res.*, 114,  
672 A07106, doi:10.1029/2008JA014034.
- 673 Russell, C. T., R. L. McPherron, and R. K. Burton (1974), On the cause of geomagnetic  
674 storms, *J. Geophys. Res.*, 79, 1105-1109.
- 675 Schmidt, J. M., and P. J. Cargill (2003), Magnetic reconnection between a mag-  
676 netic cloud and the solar wind magnetic field, *J. Geophys. Res.*, 108, 1023,

677 doi:10.1029/2002JA009325.

678 Schwartz, S. J. (1998), Shock and Discontinuity Normals, Mach Numbers, and Related Pa-  
679 rameters, In: Analysis Methods for Multi-Spacecraft Data, Gtz Paschmann and Patrick  
680 Daly (eds.), ISSI Scientific Reports Series, 1,1998, 249-270.

681 Singh, A. K., D. Singh, R. P. Singh (2010), Space Weather: Physics, Effects, and Pre-  
682 dictability, Surv. Geophys., 31, 581-638, doi:10.1007/s10712-010-9103-1.

683 Suess, S. T., Y.-K. Ko, R. von Steiger, and R. L. Moore (2009), Quiescent current  
684 sheets in the solar wind and origins of slow wind, J. Geophys. Res., 114, A04103,  
685 doi:10.1029/2008JA013704.

686 Taubenschuss, U., N. V. Erkaev, H. K. Biernat, C. J. Farrugia, C. Möst, and U. V.  
687 Amerstorfer (2010), The role of magnetic handedness in magnetic cloud propagation,  
688 Ann. Geophys., 28, 1075-1100, doi:10.5194/angeo-28-1075-2010.

689 Thernisien, A. F. R., R. A. Howard, A. Vourlidas (2006), Modeling of flux rope coronal  
690 mass ejections, The Astrophysical Journal, 652, 763-773.

691 Thernisien, A. F. R. (2011), Implementation of graduated cylindrical shell model for the  
692 three-dimensional reconstruction of coronal mass ejections, The Astrophysical Journal  
693 Supplement Series, 194, 33.

694 Tsurutani, B. T., B. E. Goldstein, W. D. Gonzalez, and F. Tang (1988), Comment on A  
695 new method of forecasting geomagnetic activity and proton showers by A. Hewish and  
696 P. J. Duffet-Smith, Planet. Space Sci., 36, 205-206.

697 Vršnak, B. et al. 2013, Propagation of interplanetary coronal mass ejections: The drag-  
698 based model, Solar Physics, 285, 295



- 699 Wang, Y., Wang, B., Shen, C., Shen, F., & Lugaz, N. 2014, Deflected propagation of a  
700 coronal mass ejection from the corona to interplanetary space, *Journal of Geophysical*  
701 *Research (Space Physics)*, 119, 5117
- 702 Winslow, R. M., N. Lugaz, L. C. Philpott, N. A. Schwadron, C. J. Farrugia, B. J. An-  
703 dersson, and C. W. Smith (2015), Interplanetary coronal mass ejections from MESSENER  
704 orbital observations at Mercury, *J. Geophys. Res. Space Physics*, 120, 6101-6118,  
705 doi:10.1002/2015JA021200.
- 706 Winterhalter, D., E. J. Smith, M. E. Burton, N. Murphy, and D. J. McComas (1994),  
707 The heliospheric plasma sheet, *J. Geophys. Res.*, 99, 6667-6680.
- 708 Zhang, J.-Ch., M. W. Liemohn, J. U. Kozyra, B. J. Lynch, and T. H. Zurbuchen (2004),  
709 A statistical study of the geoeffectiveness of magnetic clouds during high solar activity  
710 years, *J. Geophys. Res.*, 109, A09101, doi:10.1029/2004JA010410.
- 711 Zurbuchen, T. H., & I. G. Richardson 2006, In-situ solar wind and magnetic field signa-  
712 tures of interplanetary coronal mass ejections, *Space Science Reviews*, 123, 31.

**Figure 1** COR2 STEREO A (a) and B (b) white light images (at 19:08:15 on 29 Dec. 2011) with an overlay in green of the GCS wireframe. Figure credit: <http://www.affects-fp7.eu/helcats-database>.

**Figure 2** MESSENGER measurements of the ICME on 30-31 December 2011. The first four panels show magnetic field data in RTN coordinates. The last panel shows FIPS data of the proton flux over the same time period. Vertical magenta lines denote the crossing time of the ICME shock, magnetic ejecta, and ICME end. The data gap corresponds to MESSENGER's passage through Mercury's magnetosphere. For this event, the ICME end was marked by a small discontinuity or reverse shock (not visible at this scale on the figure).

Author Manuscript

**Figure 3.** STEREO A magnetic field and plasma data of the ICME on 1-2 January 2012. From top to bottom: the magnetic field magnitude, the magnetic field vector components in RTN coordinates, suprathermal electron pitch angle distributions, the proton density, velocity, temperature, the plasma  $\beta$ , and the 10-minute averaged iron charge state distribution over the time period. Vertical magenta lines denote the crossing time of the ICME shock, magnetic ejecta, and ICME end, while the black vertical lines denote the start and end of the turbulent region. The black dashed line indicates the time of the return to bi-directional electron flows in the magnetic ejecta.

**Figure 4.** STEREO A magnetic field and plasma data of the magnetic ejecta. From top to bottom: the magnetic field magnitude, the magnetic field vector components in RTN coordinates, suprathermal electron pitch angle distributions, the proton density, velocity, temperature, and the plasma  $\beta$ . The vertical black lines denote the start and end of the turbulent region, while the black dashed line indicates the time of the return to bi-directional electron flows in the ME.

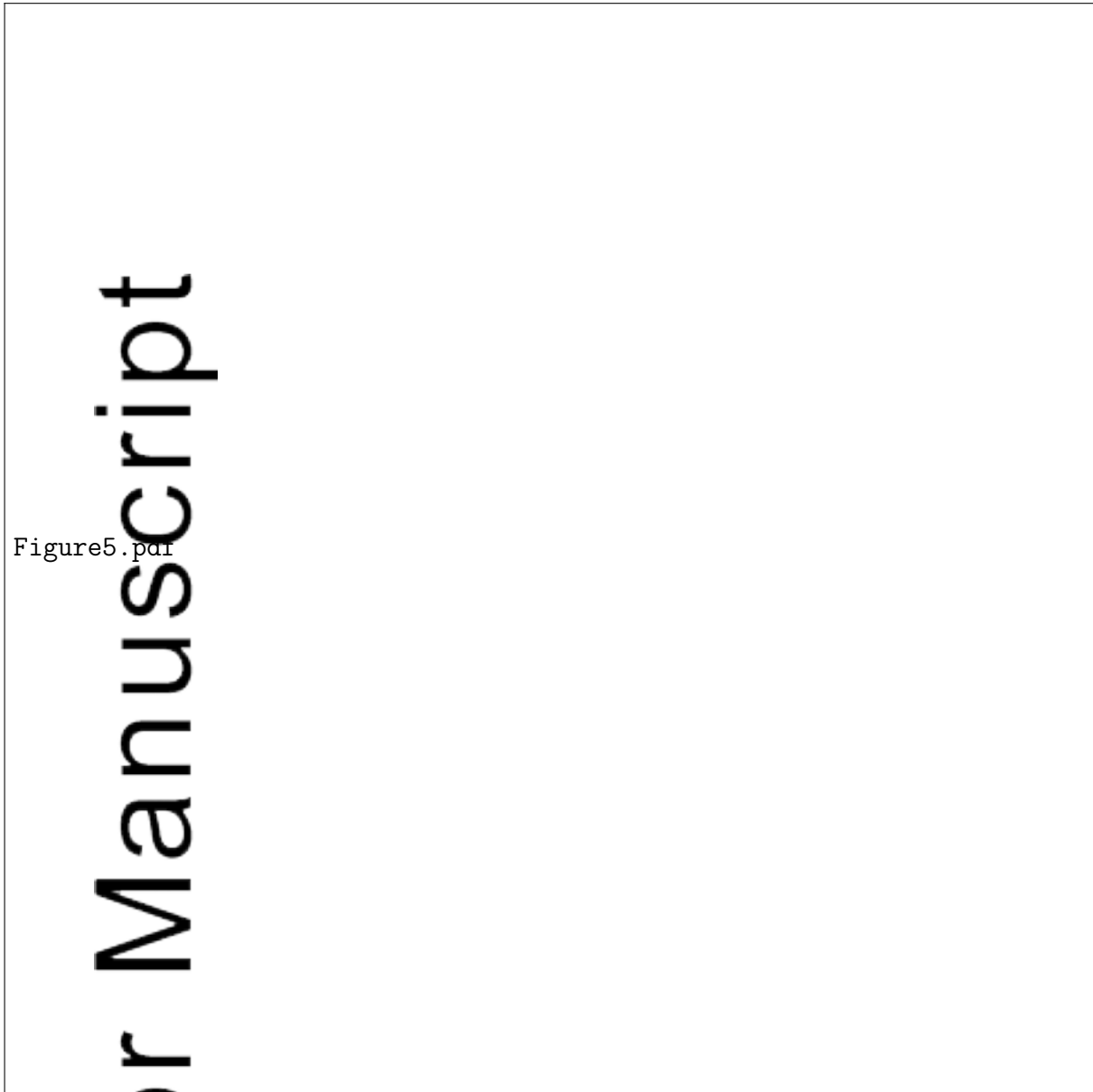


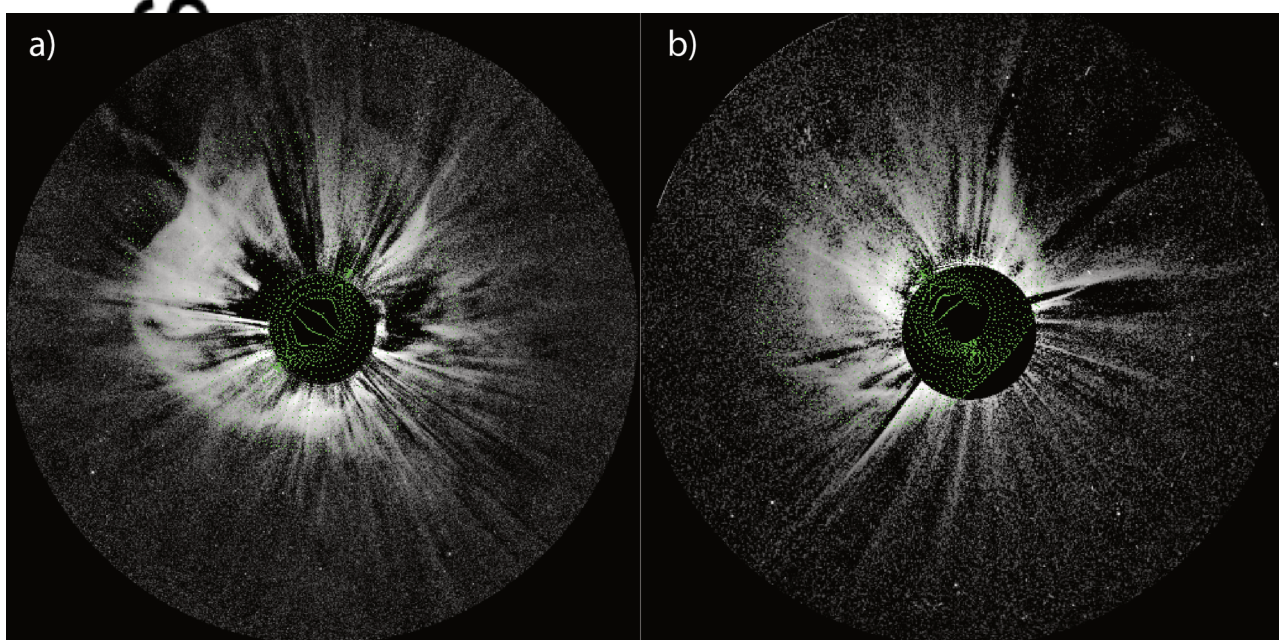
**Figure 5** Force-free field constant  $\alpha$  fits to binned MESSENGER (a) and STEREO A (b) magnetic field data. The fit results yielded left-handed flux ropes at both spacecraft, with flux rope parameters at MESSENGER of  $\theta = -12.3^\circ \pm 0.4^\circ$ ,  $\phi = 131^\circ \pm 1^\circ$ , and  $B_0 = 55.9 \pm 0.5$  nT and at STEREO A of  $\theta = 66^\circ \pm 5^\circ$ ,  $\phi = 197^\circ \pm 8^\circ$ , and  $B_0 = 12.3 \pm 0.5$  nT.

**Figure 6.** STEREO A magnetic field and plasma data a few days before and after the ICME. The panels are the same as in Figure 4, and the labeling of the vertical lines are the same as in Figure 3. The highlighted yellow region marks the beginning portion of the heliospheric plasma sheet (HPS).

**Figure 7.** Panels a-b: ENLIL-MAS model simulated steady-state solar wind conditions for two time steps: a) at 18:00 UT on 30 December 2011, just after the ICME reached MESSENGER, and at b) 12:00 UT on 1 January 2012, just before the ICME reached STEREO A. a) Shows that the HPS/HCS had passed by Mercury prior to the ICME arrival, while b) shows that the HPS/HCS is about to reach STEREO A, very close to the time that the ICME also arrived.

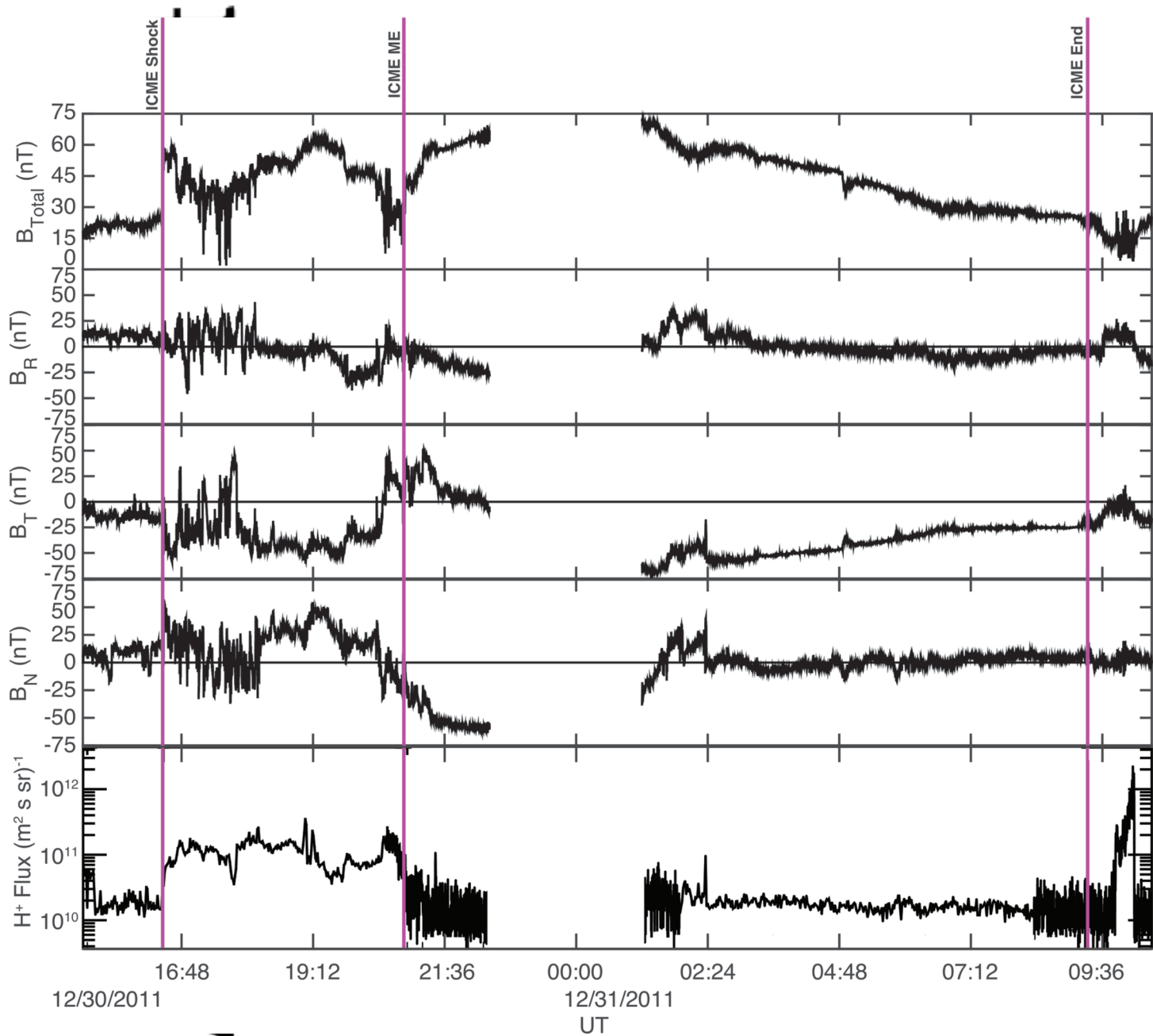
**Figure 8.** Panels a-b: Cartoon depiction of possible reconnection between the ICME flux rope and HPS field lines. After reconnection, the ICME magnetic topology is altered and some HPS plasma is now on ICME field lines.

script



2015ja022307-f01-z-.eps

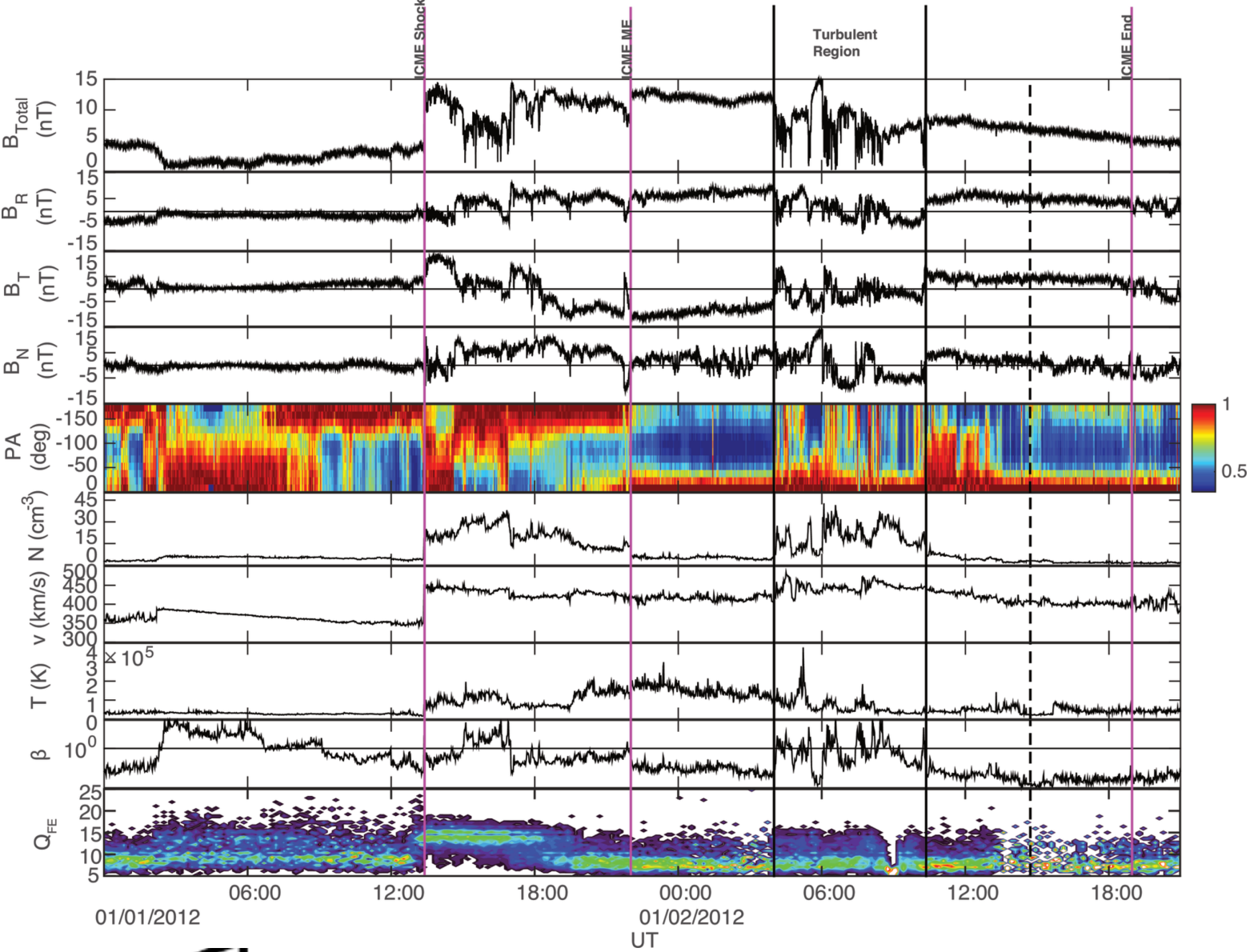
Auth



2015ja022307-f02-z-.eps

t

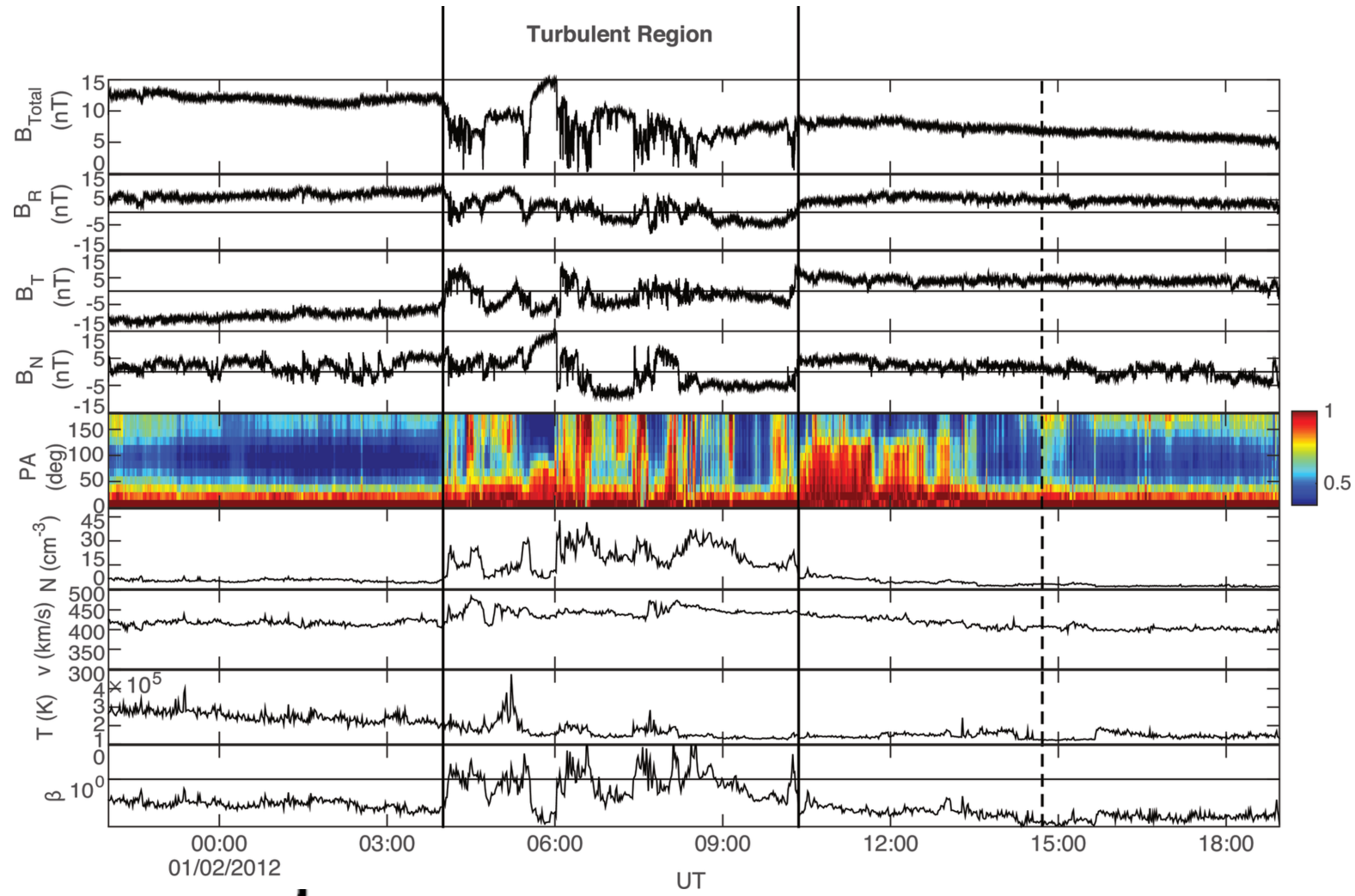
A



2015ja022307-f03-z-.eps

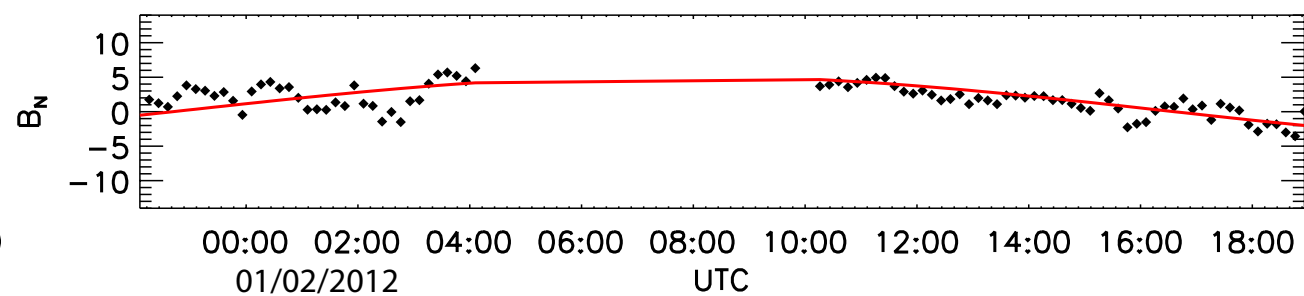
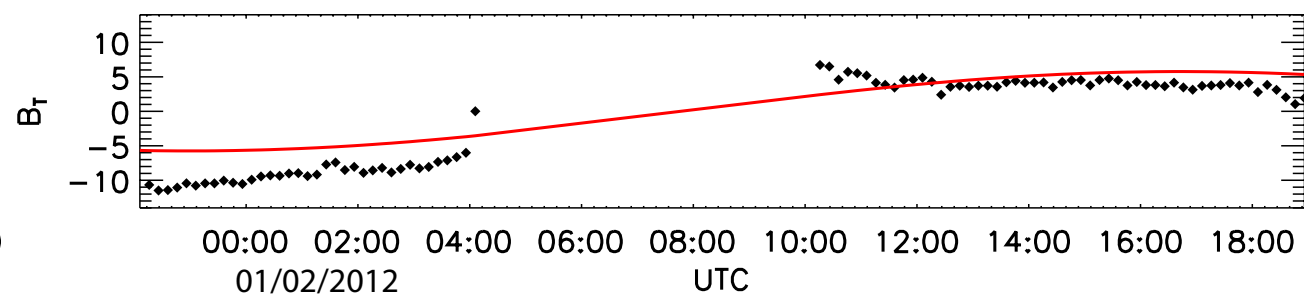
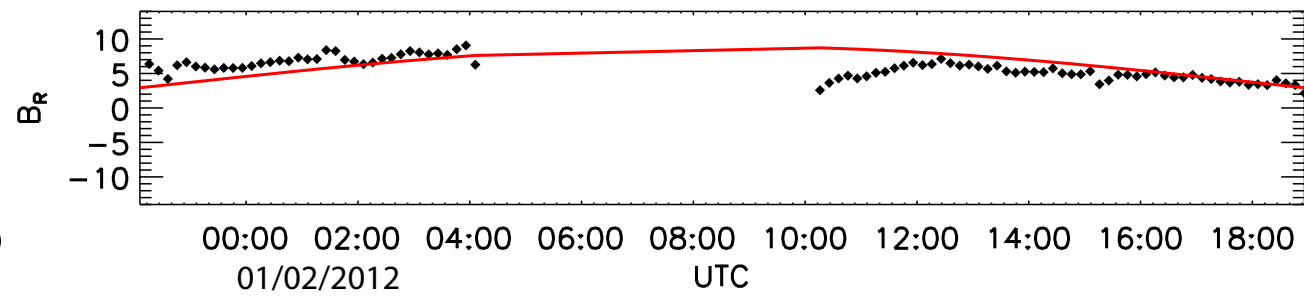
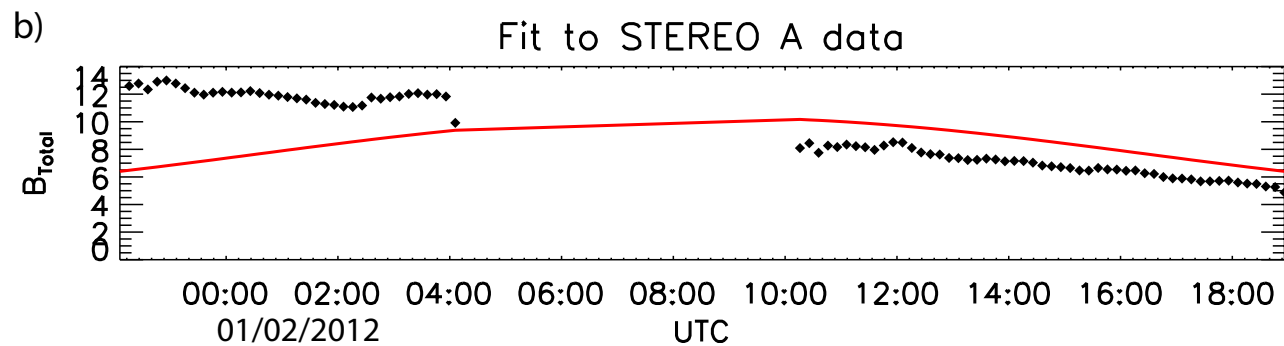
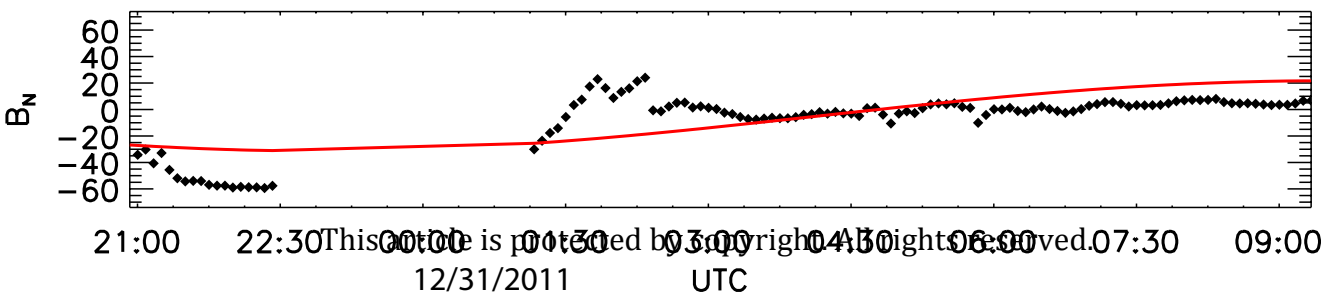
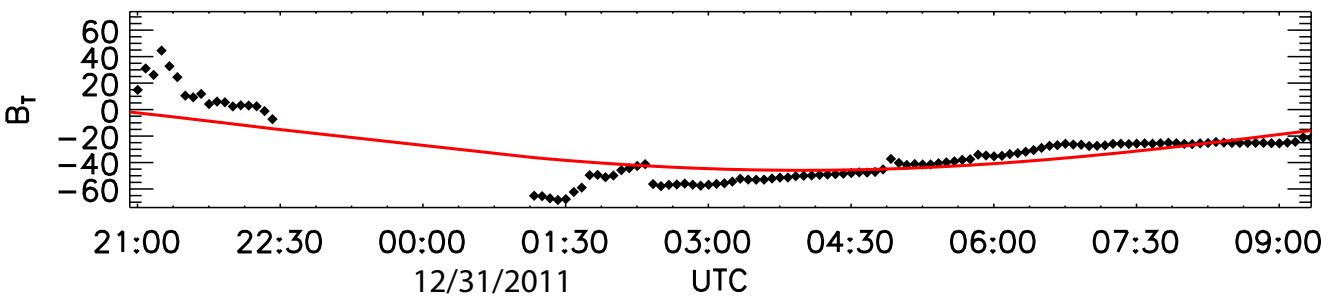
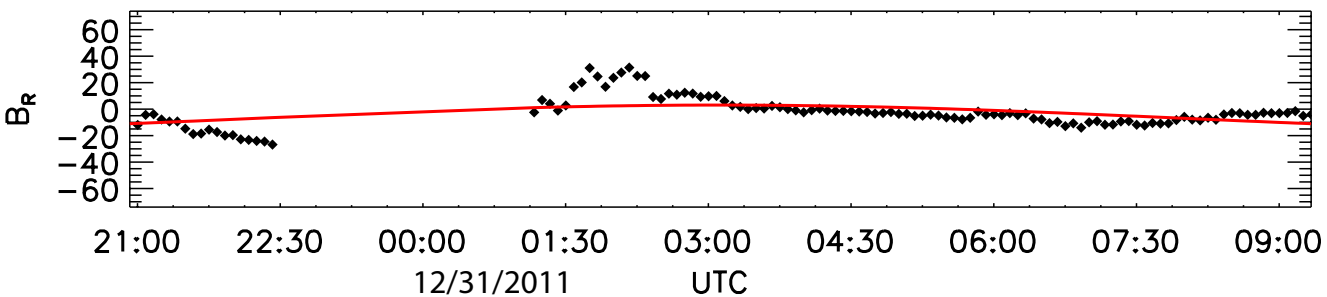
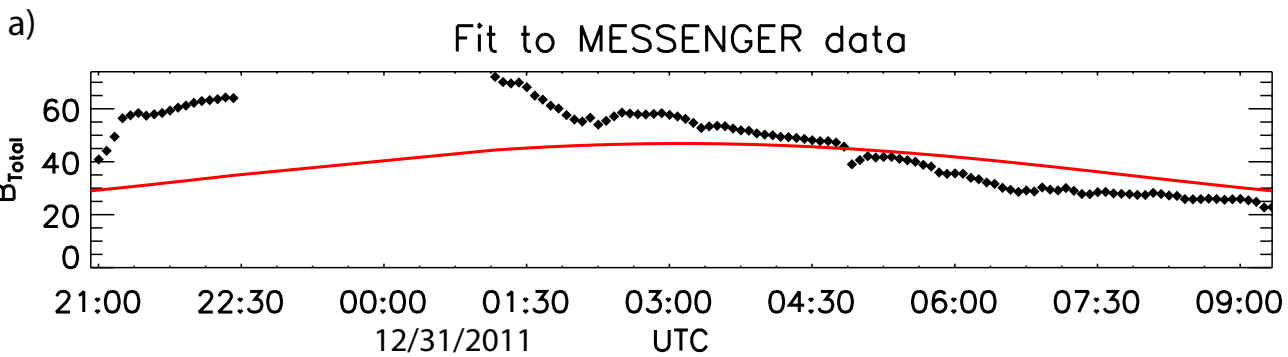


pt

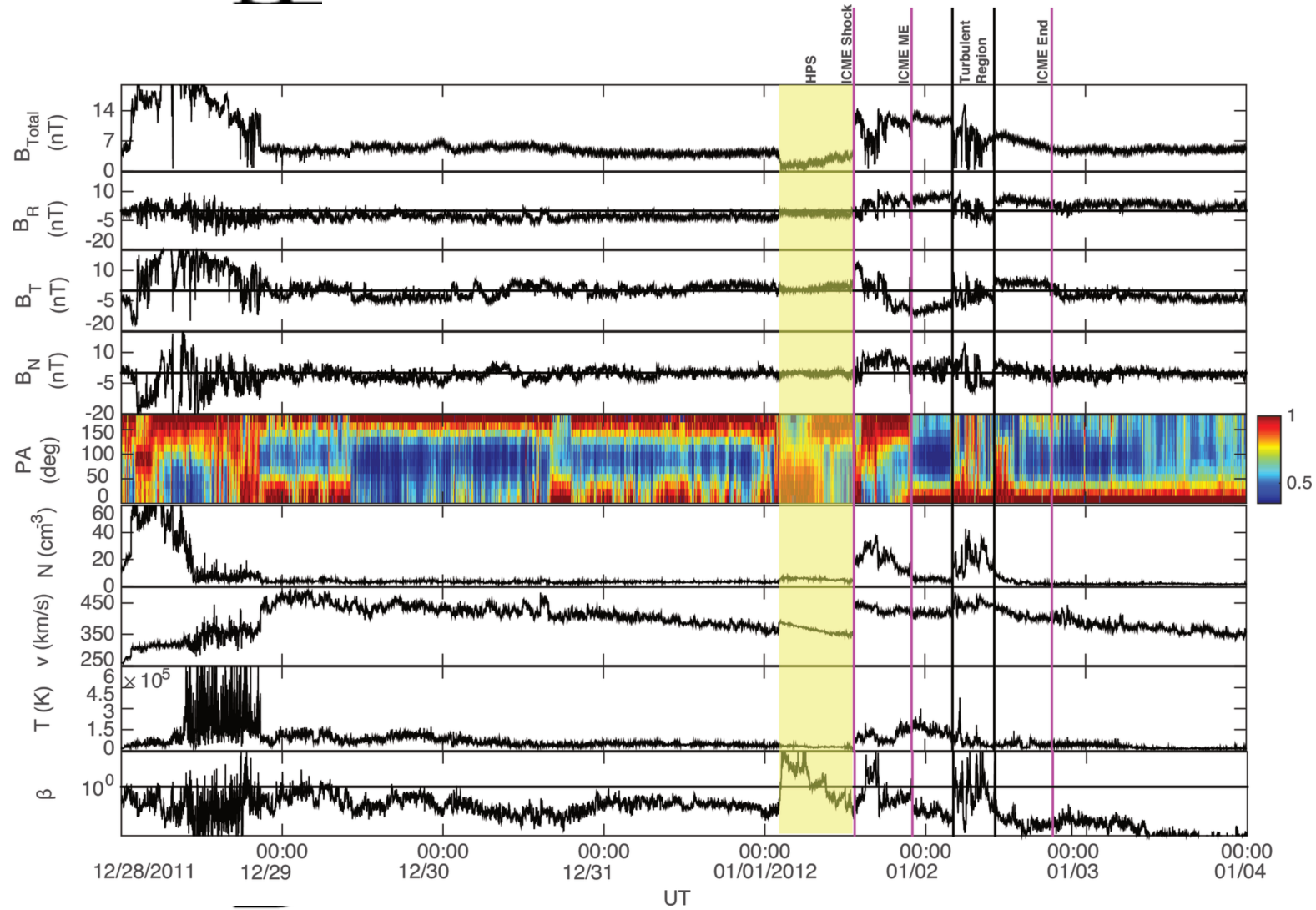


Al

2015ja022307-f04-z-.eps



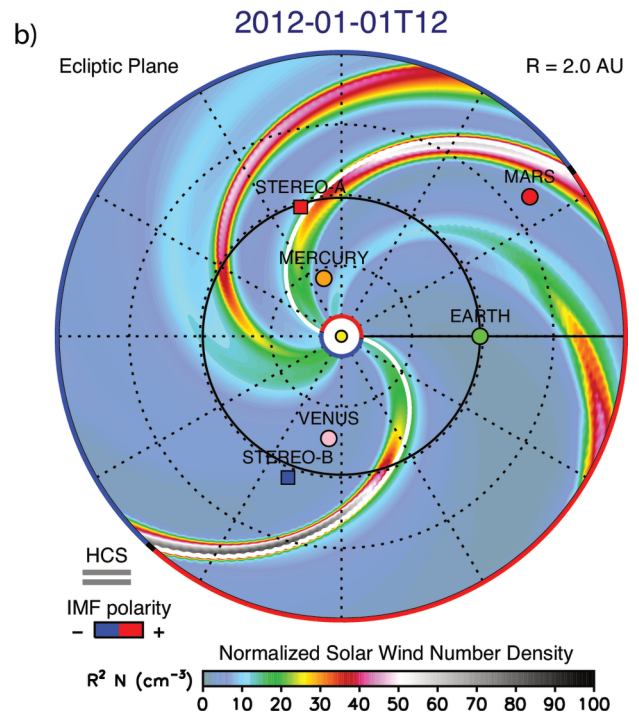
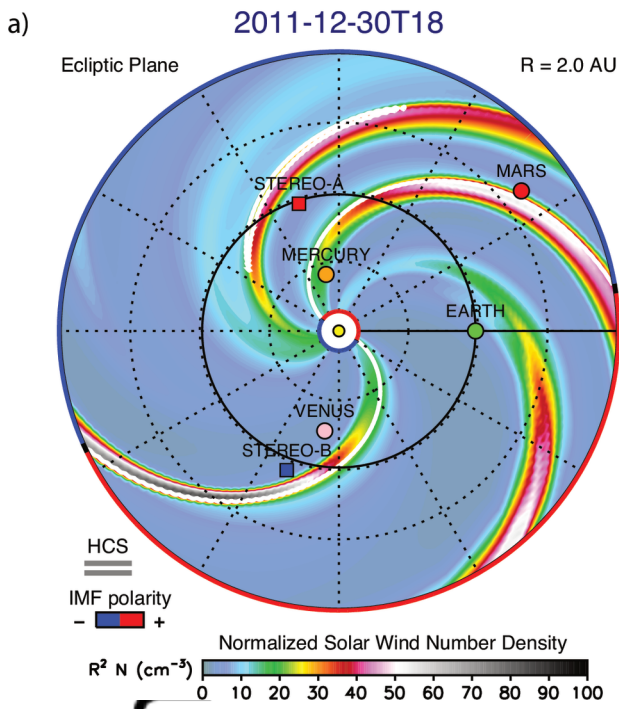
ot



A

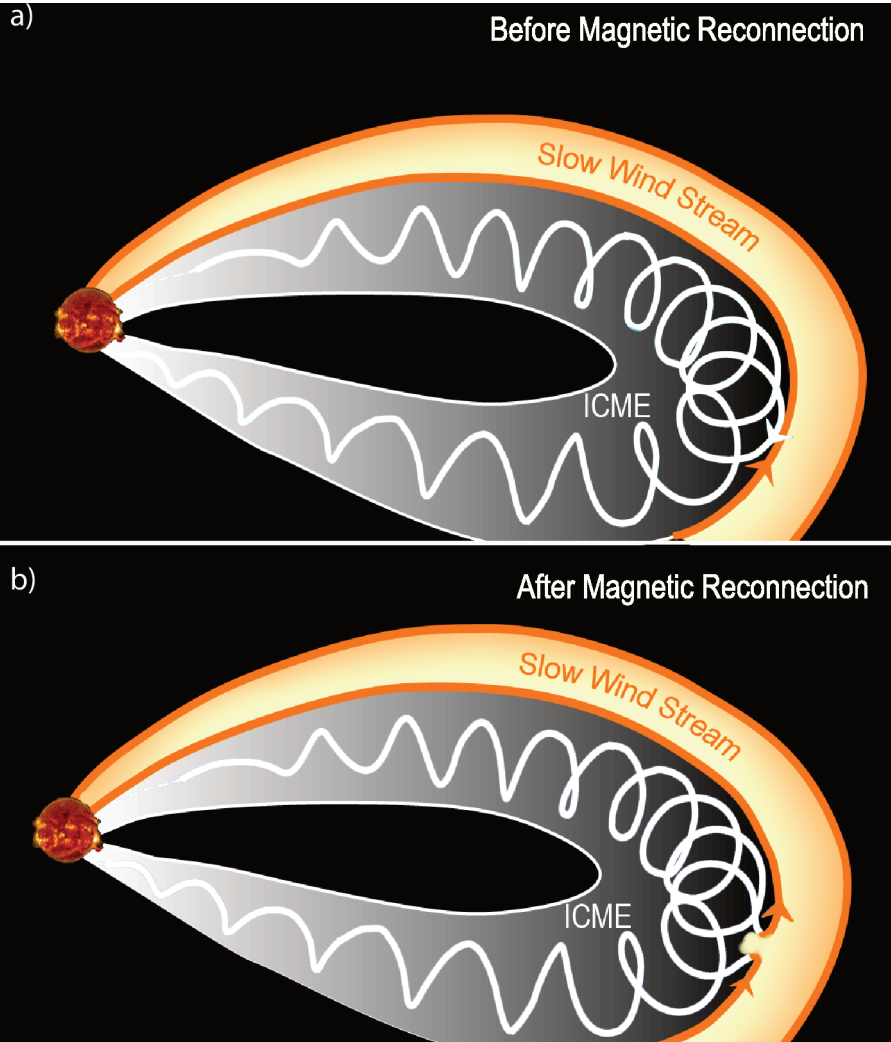
2015ja022307-f06-z-.eps

cript



Auth

2015ja022307-f07-z-eps



2015ja022307-f08-z-.eps